

Ultrafast dynamics of surface electromagnetic waves in nanohole array on metallic film

A. S. Kirakosyan,^{1,2} M. Tong,³ T. V. Shahbazyan,¹ and Z. V. Vardeny³

¹*Department of Physics, Jackson State University, Jackson, MS 39217 USA*

²*Department of Physics, Yerevan State University, Yerevan, 375025 Armenia*

³*Department of Physics, University of Utah, Salt Lake City, Utah 84112 USA*

We study the ultrafast dynamics of surface electromagnetic waves photogenerated on aluminum film perforated with subwavelength holes array by means of transient photomodulation with ~ 100 fs time resolution. We observed a pronounced *blueshift* of the resonant transmission band that reveals the important role of plasma attenuation in the dynamics and that is inconsistent with plasmon-polariton mechanism of extraordinary transmission. The transient photomodulation spectra were successfully modeled within the Boltzmann equation approach for the electron-phonon relaxation dynamics, involving non-equilibrium hot electrons and quasi-equilibrium phonons.

I. INTRODUCTION

On a smooth metal-dielectric interface light does not couple to elementary electronic excitations of the metal surfaces because of energy and momentum conservation. But in a metal film that is perforated with a two-dimensional (2D) periodic array of holes forming a 2D metallo-dielectric photonic crystal, the periodicity promotes zone folding that results in the formation of band structure. The grating makes it possible for light to couple directly to surface electromagnetic waves by transferring them the reciprocal lattice momentum $g = 2\pi/a$, where a is the grating period¹. Indeed, it was recently found^{2,3,4} that the optical transmission through hole arrays fabricated on optically thick metallic films is enhanced by orders of magnitude at resonances; this phenomenon has been dubbed "extraordinary transmission" (EOT). The maxima in the zero-order transmission spectrum is alternated by deep minima caused by Wood's anomalies formed due to the diffraction grating of the corrugated film. The optical properties of various subwavelength hole array films have been widely studied and different models have been proposed to explain the underlying mechanism of the anomalous transmission. While earlier models attributed the enhancement to excitation of film's surface plasmon-polaritons (SPP)^{2,3,4,5,6}, more recent works addressed the role resonant cavity modes^{7,8,9}, dynamical diffraction resonances^{10,11}, and interference of diffracted evanescent waves¹². While the precise mechanism of extraordinary transmission is still under discussion, the transient dynamics of surface electromagnetic modes might shed more light on the origins of this phenomenon.

Here we investigate the ultrafast dynamics of surface electromagnetic modes measured by using the pump-probe correlation spectroscopy of the transmission bands in 2D subwavelength hole array on aluminum (Al) thin film. We found significant difference with the dynamics observed previously in smooth metal films (mostly gold and silver) in both the time-resolved and spectrally-resolved signals. Following an instantaneous rise at the onset of the impinging pulse, the transient differential transmission exhibits a fast rise on subpicosecond

timescale followed by a plateau for time delays of 1-3 ps, and subsequent slow decay with characteristic time of ~ 40 ps. The short-time dynamics is accompanied by a blueshift of the main transmission band in the transient spectra that persists for time delays as long as 100 ps. The observed dynamics can be explained by a fast energy transfer in the Al film from the electron gas to the lattice, with subsequent cooling of the Al film by heat transfer to the glass substrate. The fast lattice temperature rise is caused by strong electron-phonon interaction in Al, which makes the electron-lattice energy transfer rate comparable to the rate of nonequilibrium electrons thermalization via electron-electron interactions¹³. Importantly, the blueshift is inconsistent with the SPP mechanism and points to the interference as the source of the extraordinary transmission.

II. EXPERIMENT

The plasmonic lattice sample was a 70 nm thick Al film, 5×5 mm² in area deposited on a glass substrate. The metal film was perforated with circular holes having diameter $D = 150$ nm in a square hole array with lattice constant $a = 300$ nm resulting in a fractional aperture area of 25%. The ultrafast laser system used for measuring the transient PM spectrum was a Ti:sapphire regenerative amplifier with pulses of 100 fs duration at photon energies of 1.55 eV, with 400 μ J energy per pulse at a repetition rate of 1 kHz. The second harmonic of the fundamental pulses at 390 nm (3.1 eV) were used as the pump beam. The probe beam was a white light supercontinuum generated in a 1-mm thick sapphire plate that covers the spectral range from 1.6 to 2.8 eV; the white light supercontinuum was also used for measuring the unperturbed transmission spectrum $T_0(\omega)$. The pump and probe beams were directed onto the perforated Al film from the air side to maximize coupling of light to the SEW. The transient PM spectrum was obtained from the photoinduced change (ΔT) in T_0 using a phase-sensitive technique with a resolution $\Delta T/T_0 \sim 10^{-4}$ that corresponds to a photoexcited electron density in the Al metal of $\sim 10^{17}$ cm⁻³/pulse.

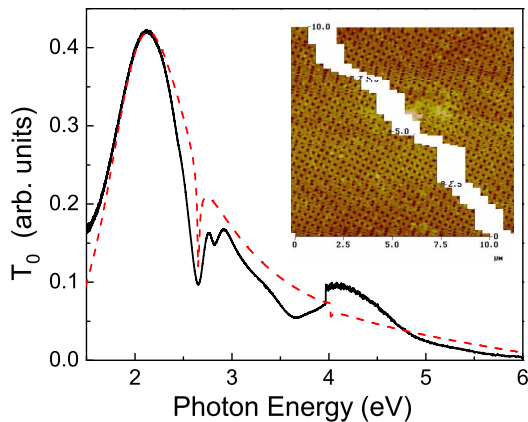


FIG. 1: The measured (solid line) and calculated (dashed line) normal incidence optical transmission, T_0 through an Al plasmonic lattice comprised of a square array of nanoholes with lattice constant 300 nm and hole diameter 150 nm. The inset shows the sample AFM image. Numerical fit is based on the effective medium model for linear transmission in Sec. III A.

Figure 1 shows the EOT spectrum of the Al plasmonic lattice at normal incidence. Several EOT bands and transmission anti-resonances (AR) are observed. We note that $T_0(\omega)$ at resonance frequencies substantially surpasses the fractional aperture area of 25%. The lowest frequency EOT band peaks at ~ 2.1 eV; whereas the lowest frequency AR feature that is associated with Wood's anomaly at the Al/glass interface with wavevector $k^{(01)} = g\varepsilon_{gl}^{-1/2}$ (where $\varepsilon_{gl} = 1.56$ and $g = 2\pi/a$) is in the form of a dip at 2.6 eV. The AR's at higher frequencies are higher-order Wood's anomalies that correspond to wavevectors $k^{(mn)} = g(m^2 + n^2)^{1/2} \varepsilon_d^{-1/2}$ (m, n are integers) as follows: 3.7 eV ($k^{(11)} = g\varepsilon_{gl}^{-1/2} 2^{1/2}$) that corresponds to the (1,1) branch at the Al/glass interface; and 4.0 eV ($k^{(01)} = g$) that corresponds to the (0,1) branch at the Al/air interface. It is noteworthy that the lowest frequency EOT resonance (at ~ 2.1 eV) occurs at considerably lower (by ~ 0.6 eV) frequency than that predicted by the lowest-order SPP with wavevector satisfying the Bragg condition²

$$k_{spp}^{(mn)} = g [(m^2 + n^2) (\varepsilon_m^{-1} + \varepsilon_d^{-1})]^{1/2}. \quad (1)$$

The transient PM spectra of the perforated Al film are shown in Figs. 2 - 4. The time-evolution of pump-probe signal at 650 nm, corresponding to probe photon energy of 1.9 eV, reveals two component of the dynamics. Firstly, there is a fast rise of pump-probe signal on timescale < 1 ps, followed by a plateau at 1-3 ps (see Fig. 2). Secondly, after about 3 ps the saturated PM decays with characteristic time of ~ 40 ps (see Fig. 3) due the heat transfer to the glass substrate. Figure 4(a) shows the transient PM spectral change from 1.7 to 2.4 eV corresponding roughly to the main transmission band spec-

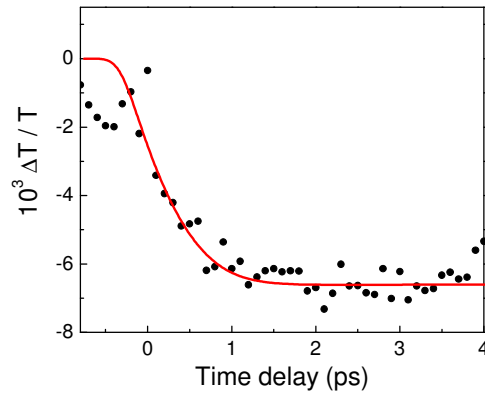


FIG. 2: Short-time evolution of differential transmission at 1.9 eV is shown together with numerical fit (solid line) based on solution of the Boltzman equation in Sec. III B.

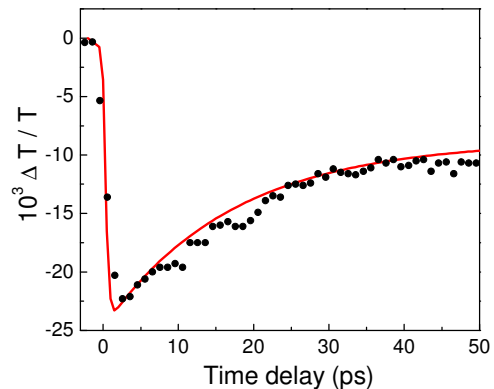


FIG. 3: Long-time evolution of differential transmission at 1.9 eV due to heat transfer to the glass matrix is shown together with numerical fit (solid line) based on two-temperature model in Sec. III B.

tral width. A transient blueshift is apparent that persists for times up to 100 ps, i.e. much longer than electron gas thermalization time, pointing to a prominent role of e - ph interactions in the dynamics. However this shift cannot be well reproduced by a simple spectral derivative [see Fig. 4(b)] indicating that a perturbation approach cannot properly describe the observed changes in optical spectra for our excitation intensities. At the same time, although the data becomes more noisy at higher energies as one approaches to the Wood anomaly, a clear nonlinearity in the frequency dependence emerges. The energy dependence of dT/T is determined by transient change in the mode dispersion that reflects the periodicity of the structure.

The short-time dynamics exhibits significant differences with that observed in gold and silver films^{14,15}. In these studies, the picosecond dynamics consisted of two well-separated in time stages: thermalization of nonequilibrium electrons due to electron-electron (e - e) scattering at 200-500 fs accompanied by the signal rise, followed

by the decay on a 1-2 ps timescale due to the cooling of hot electron gas to the metal lattice. The dominant factor that determines the transient dynamics in noble metals is the change in the interband susceptibility of the highly polarizable d -band electrons that is very sensitive to the smearing of the Fermi edge due to the rise in electron temperature T_e . In contrast, in simple metals such as Al, the transient optical spectra are governed by the changes in the intraband dielectric function $\varepsilon_m(\omega) = 1 - \omega_p^2/\omega(\omega + i\gamma)$, where ω_p is the bulk plasmon energy and γ is the optical relaxation rate¹⁶. The absorbance of the film and hence the transient dynamics is related to the deviation of γ from its intrinsic value γ_0 that mainly originates from the change in the electron-phonon (e - ph) scattering, while the contributions from e - e , and impurity scattering are relatively weak¹⁷. Note that the e - ph interaction constant G in Al is an order of magnitude larger than it is in noble metals (for comparison, $G_{Al} = 3.1 \times 10^{17}$ W/Km³ vs. $G_{Au} = 2 \times 10^{16}$ W/Km³), so that the energy exchange between the electron and phonon subsystems takes place on sub-picosecond times¹⁸. The rapid increase in the lattice temperature T_L and hence in the e - ph relaxation rate accounts for the fast rise of the pump-probe signal until the equilibrium between electron and phonon subsystems is reached at ~ 1 ps. This fast dynamics is superimposed with a slow decay due to the heat transfer from metal to glass substrate resulting in a plateau at 1-3 ps (see Figs. 2-3). Importantly, the merging of electron thermalization and electron to lattice cooling stages implies that the short time dynamics is intrinsically nonequilibrium; it is therefore described below within the Boltzmann equation approach.

The observed PM blueshift also indicates that the EOT is sensitive to the imaginary part of permittivity, $\varepsilon_m''(\omega)$, for the following reason. Within the Drude model for Al, we have $\varepsilon_m'(\omega) = 1 - \omega_p^2/(\omega^2 + \gamma^2)$. With such ε_m' , the SPP Bragg condition Eq. (1) leads to the following expression for, e.g., (0,1) mode frequency (at $\epsilon_d = 1$): $\omega_{spp}^{01} \approx \omega_g [1 - (\omega_g^2 + \gamma^2)/2\omega_p^2]$, where $\omega_g = cg$ is the frequency associated with the reciprocal lattice period. Then an increase in γ upon pulsed excitation leads to a weak redshift of the resonance frequency, in disagreement with the data. We thus conclude that the observed spectral blueshift cannot be explained by the present version of the SPP mechanism for the EOT phenomenon². At the the same time, an increase in γ causes an increase in the *attenuation*, ε_m'' , which for $\gamma \ll \omega$ can be approximated by $\varepsilon_m'' \approx \gamma\omega_p^2/\omega^3$. If ε_m'' participates in determining the position and lineshape of the EOT bands, then the increase in γ implies *higher* resonant frequencies (blueshift) in agreement with the data. The linear transmission is modeled below using effective medium approach.

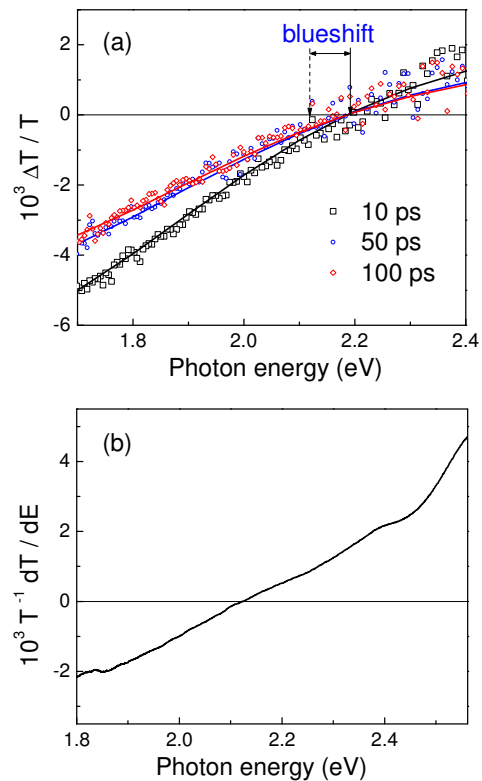


FIG. 4: (a) Transient spectra at different time delays are shown together with numerical fit (solid lines) based on solution of the Boltzman equation in Sec. III B. (b) Log derivative of measured zero-order transmission.

III. THEORY

The transient optical spectra in metal films can be described in terms of time-dependent dielectric function $\varepsilon_m(\omega, t) = \varepsilon_m(\omega) + \delta\varepsilon_m(\omega, t)$, where $\varepsilon_m(\omega, t)$ is PM contribution due to a small (compared to ground state) fraction of photoexcited carriers. The differential transmission $\Delta T(t) = T(t) - T_0$ can be then calculated from the linear transmission $T_0(\omega)$ with $\varepsilon_m(\omega, t)$ ^{14,15}. While the time-resolved signal is primarily governed by the electron dynamics in metal film encoded in $\delta\varepsilon_m(\omega, t)$, the transient *spectra* are determined by the effect of the latter on the *dispersion* of surface electromagnetic modes. Modeling of the dynamics thus involves two distinct tasks: (i) description of the linear transmission through nanohole array for *real* metal with absorptive dielectric function, and (ii) simulation of non-equilibrium electron-phonon dynamics in Al film.

A. Effective medium model for linear transmission

We begin with *analytical* model for the main transmission band that incorporates the effect of the absorptive part of metal dielectric function. We are interested in the transmission of p -polarized light normally incident

on a metal film perforated with square array of cylindrical nanoholes. We assume that the scattering in the direction normal to the plane of incidence is weak and adopt one-dimensional grating approximation for transverse magnetic and electric fields, $H_y(x, z)$ and $E_x(x, z)$. Magnetic fields in air (media 1), perforated metal (media 2), and glass (media 3), can be written as

$$H_{1y} = e^{ik_1z} + \sum_n r_{1n} e^{-ik_{1n}z + ingx}, \quad (2)$$

$$H_{3y} = \sum_n t_{3n} e^{ik_{3n}(z-h) + ingx}, \quad (3)$$

$$H_{2y} = \sum_i H_i(x) \left[t_{2i} e^{-\kappa_i z} + r_{2i} e^{-\kappa_i(h-z)} \right], \quad (4)$$

where $k_{jn} = \sqrt{k_0^2 \epsilon_j - n^2 g^2}$ and $k_j \equiv k_{j0}$ (here $k_0 = \omega/c$), and r_{jn} , and t_{jn} are reflection and transmission amplitudes of order n in medium j respectively ($j = 1, 3$). In air/glass, the fields are expanded in the Bloch functions basis. In the medium 2 (perforated metal), the expansion goes over the normalized eigenstates of Maxwell equations (ME) in periodic medium, $H_i(x)e^{-\kappa_i z}$, where eigenvalue κ_i is the wave-vector along the normal to the surface. The eigenfunctions $H_i(x)$ are localized in the hole region and are periodic over the array. The transverse electric fields in all three media are expressed through transverse magnetic fields via ME $E_x = -(i/k_0 \epsilon) \partial H_y / \partial z$. In the relevant spectral range, it is sufficient to restrict to the lowest modes in air/glass ($n = 0, \pm 1$), and in perforated metal $i = 1$.

The transmission coefficient is obtained by matching transverse electric and magnetic fields at air/metal and metal/glass interfaces. It is convenient to perform this matching in the Bloch basis for electric field, and in the basis of eigenstates H_i for magnetic field. This choice takes into account the fact that, for low volume fraction of holes, $\nu = \pi d^2 / 4a^2 \ll 1$, the electric field is mostly reflected back into the air at the air/metal interface and transmitted to the glass at the metal/glass interface, while the magnetic field, conversely, mostly penetrates into the metal at the air/metal interface, and gets reflected back into the metal from the metal/glass boundary. We define magnetic and electric field moments averaged over the Brillouin zone (BZ) as

$$\begin{aligned} h_{in} &= \langle e^{ingx} H_i \rangle_{BZ}, \\ e_{in} &= \langle e^{ingx} E_i \rangle_{BZ} = \frac{i\kappa_i}{k_0} \left\langle e^{ingx} \frac{H_i(x)}{\epsilon_2(x)} \right\rangle_{BZ}, \end{aligned} \quad (5)$$

where $\epsilon_2(x) = \epsilon_m + (\epsilon_h - \epsilon_m)\theta_H(x)$ is periodic dielectric function, ϵ_m (ϵ_h) being dielectric function in metal (hole) region, and θ_H is the periodic step-function vanishing outside the holes. Because we consider only the fundamental mode, we drop index i hereafter. By performing matching procedure at the interfaces $z = 0$ and

$z = h$ we obtain the following system of equations

$$\begin{aligned} t_2 + r_2 u &= h_0(1 + r_{10}) + 2h_1 r_{11} \\ e_n(t_2 - r_2 u) &= \frac{k_{1n}}{\epsilon_1 k_0} (\delta_{n0} - r_{1n}), \\ t_2 u + r_2 &= h_0 t_{30} + 2h_1 t_{31}, \\ e_n(t_2 u - r_2) &= \frac{k_{3n}}{\epsilon_3 k_0} t_{3n}, \end{aligned} \quad (6)$$

with $u = e^{-\kappa z}$, yielding the zero-order transmission

$$T_0 = |t_{30}|^2 = \left| \frac{t_{12} t_{23} e^{-\kappa h}}{1 + r_{12} r_{23} e^{-2\kappa h}} \right|^2, \quad (7)$$

where $t_{12} = 2\tilde{n}_2 / (\tilde{n}_1 + \tilde{n}_2)$, $t_{23} = 2n_3 / (\tilde{n}_2 + \tilde{n}_3)$ are effective transmission amplitudes through the air/metal, and metal/glass interfaces respectively, and $r_{12} = (\tilde{n}_2 - \tilde{n}_1) / (\tilde{n}_1 + \tilde{n}_2)$, $r_{23} = (\tilde{n}_3 - \tilde{n}_2) / (\tilde{n}_2 + \tilde{n}_3)$ are the corresponding effective reflection amplitudes. The effective refraction indices \tilde{n} are given by

$$\begin{aligned} \tilde{n}_2 &= (h_0 e_0)^{-1}, \\ \tilde{n}_j &= n_j \left(1 + \frac{2h_1 \epsilon_1 k_j}{h_0 e_0 k_{j1}} \right), \end{aligned} \quad (8)$$

where n_j are refraction indices in air/glass ($j = 1, 3$). The transmission coefficient is thus expressed via the *overlap integrals*, h_n and e_n , between eigenstates in the periodic medium and in the air/glass. Such overlap causes hybridization of the states in perforated metal via the EM waves at the interfaces (both propagating and evanescent). It is this hybridization that determines the position and the lineshape of the transmission peak.

In order to proceed further, we need to evaluate the overlap integrals, h_n and e_n , and the eigenvalue κ . The former can be determined from the following self-consistency argument. While in the bulk of perforated metal the states H_i are strongly localized within holes, near the interfaces (where the overlap integrals are calculated) these states become delocalized due to the hybridization via EM in the dielectric. In other words, in the close vicinity of the interface, the profile of transverse magnetic field (that is continuous together with its derivative across the interfaces) is similar at the both sides of the interface and can be approximated as $H(x) = h_0 + 2h_1 \cos gx$. The relation between h_0 and h_1 on the metal side can therefore be determined from ME for $H(x)$,

$$\epsilon_2 \frac{\partial}{\partial x} \left(\frac{1}{\epsilon_2} \frac{\partial H}{\partial x} \right) + (k_0^2 \epsilon_2 + \kappa^2) H = 0, \quad (9)$$

with periodically modulated dielectric function, $\epsilon_2(x) = \epsilon_0 + 2\epsilon_1 \cos gx$, where $\epsilon_0 = \epsilon_m(1 - \nu) + \epsilon_h \nu$ is the average and $\epsilon_1 = \nu(\epsilon_h - \epsilon_m)\xi_1$, with $\xi_n = \sin(ngd/2)/(ngd/2)$, is the modulation amplitude¹⁹. In the first order in modulation, we obtain

$$\frac{h_1}{h_0} = -\frac{2k_0^2 \epsilon_1}{k_0^2 \epsilon_0 + \kappa^2 - g^2}, \quad (10)$$

where h_0 is determined from the normalization condition. The moments of electric field, e_n , are straightforwardly calculated from Eq. (5) as

$$\begin{aligned} e_0 &= i\kappa(h_0\tilde{\epsilon}_0 + 2h_1\tilde{\epsilon}_1)/k_0 \\ e_1 &= i\kappa[h_0\tilde{\epsilon}_1 + h_1(\tilde{\epsilon}_0 + \tilde{\epsilon}_2)]/k_0, \end{aligned} \quad (11)$$

where $\tilde{\epsilon}_n \equiv \langle e^{ingx}/\epsilon_2(x) \rangle_{BZ} = (\epsilon_h^{-1} - \epsilon_m^{-1})\nu\xi_n$.

Let us now turn to evaluation of the wavevector κ that represents the lowest eigenvalue of ME Eq. (9). The eigenvalues are determined by the bulk states of the optically thick perforated metal film, and therefore are only weakly affected by the interfaces. In the bulk, the eigenstates are strongly localized within the holes and the weakly-modulated medium approximation does not apply. In this case, the eigenvalues can be evaluated by using the analogy between ME and Schrödinger equation (SE) with complex potential. Namely, for each region, Eq. (9) can be presented in the form $\partial^2 H/\partial x^2 + (E - V)H = 0$, where

$$\begin{aligned} E &= \kappa^2 + k_0^2[\epsilon(\omega) - \epsilon_h], \\ V(x) &= k_0^2 \sum_n [\epsilon(\omega) - \epsilon_h] \theta(d/2 - |x + na|), \end{aligned} \quad (12)$$

are the energy and potential, respectively. The latter is Kronig-Penney type attractive potential of periodically spaced quantum wells. Note that $E = -k_0^2\epsilon_h$ corresponds to $\kappa^2 = -\epsilon_m k_0^2$ that is the value of κ for a solid metal film. The fundamental mode is associated to the ground state of Eq. (12) with the energy spectrum being a band with the width determined by the tunnel transparency between the wells. In the case of high metal/dielectric contrast of ϵ , so that $k_0 a \sqrt{|\epsilon_h - \epsilon_m|} \gg 1$, this transparency is exponentially small and the ground state energy can be approximated by that of the lowest level in a single well. The latter can be found by replacing rectangular well by the delta-function potential, $V(x) = V_0\delta(x)$, with the strength $V_0 = \nu(\epsilon_m - \epsilon_h)k_0^2 a$, where we averaged over BZ. We then obtain $E = -V_0^2/4$, yielding $\kappa^2 = -\epsilon_m k_0^2 - \nu^2 a^2 k_0^4 (\epsilon_m - \epsilon_h)^2/4$.

We thus arrive at the following physical picture for the main transmission band. Diffraction on an individual hole can be viewed as scattering on the bound state in the associated SE. The interference of diffracted waves, caused by the hybridization of localized hole states via EM waves in dielectrics, leads to the single-period modulation of magnetic field profile at the interfaces. The latter is determined by the *effective medium* characterized by weakly-modulated dielectric function depending on the hole volume fraction ν . Note that eigenvalue κ as well as magnetic/electric field moments h_n, e_n are complex due to absorptive part of metal dielectric function $\epsilon_m = \epsilon'_m + i\epsilon''_m$.

In Fig. 1 we show the fit of linear transmission obtained using the Drude form of dielectric function of Al, ϵ_m , with bulk plasmon frequency $\omega_p = 15.0$ eV and damping rate $\gamma = 0.2$ eV¹⁶. It can be seen that the main transmission

band is described accurately, including the position of Wood's anomaly at $\omega \approx 2.6$ eV. Higher order maxima, including possible SPP peak at 4.0 eV are not captured within this model.

B. Ultrafast Dynamics

We now turn to the modeling of ultrafast dynamics. The transient spectra in a perforated film can be obtained from the linear transmission $T_0(\omega)$ by the replacement $\epsilon_m(\omega) \rightarrow \epsilon_m(\omega) + \delta\epsilon_m(\omega, t)$, where $\delta\epsilon_m(\omega, t)$ is the non-equilibrium contribution to the metal dielectric function. As noted above, $\delta\epsilon_m(\omega, t)$ is mainly due to transient change in the *e-ph* relaxation rate $\gamma(t)$ in the Drude dielectric function. The distinctive feature of electron dynamics in Al films is a very fast (hundreds of fs) energy exchange between electron and phonon subsystems caused by strong *e-ph* interaction in Al. This energy exchange takes place on the same timescale as the electron gas thermalization due to *e-e* scattering, rendering the transient dynamics inherently non-equilibrium. Note however that the high-energy fraction of photoexcited electrons with the excess energy $(E - E_F) \sim \hbar\omega$, scatter down on the timescale of tens of fs due to the quadratic energy dependence of *e-e* scattering rate, $\gamma_{ee} \propto (E - E_F)^2$, whereas the thermalization of electron population is reached on the longer timescale of hundreds of fs¹⁴. Therefore, the higher energy end of electron distribution relaxes primarily via *e-e* scattering processes while the energy transfer to the phonons primarily goes through the lower energy electrons. Since the overall heating of the lattice is of the order of Debye temperature ($\Theta_D \approx 380$ K in Al), the phonons that gain energy from athermal electron gas can be considered as quasi-equilibrium. The energy exchange between phonon and electron subsystems can be then described in terms of time-dependent lattice temperature $T_L(t)$ as

$$C_L \frac{\partial T_L}{\partial t} = - \int dE g(E) E \left(\frac{\partial f}{\partial t} \right)_{e-ph}, \quad (13)$$

where C_L is the lattice heat capacity ($C_L = 900$ J/Kkg for Al), $g(E) = E^{1/2}(2m_e)^{3/2}/2\pi^2\hbar^3$ is the electron density of states (DOS), and $f(E, t)$ is the electron distribution function that satisfies the Boltzmann equation

$$\frac{\partial f}{\partial t} = \left(\frac{\partial f}{\partial t} \right)_{e-e} + \left(\frac{\partial f}{\partial t} \right)_{e-ph} + H(E, t). \quad (14)$$

Here the first two terms in r.h.s. are due to *e-e* and *e-ph* scattering processes respectively, and $H(E, t)$ stands for electron-gas excitation by the pump pulse. Naturally, only the *e-ph* scattering term contributes to the energy exchange rate Eq. (13). Since the typical phonon energy is much smaller than the electron energy, the *e-ph* term can be more conveniently presented in the differential operator form²⁰. In the deformation potential approxi-

mation, the e - ph scattering term reads

$$\left(\frac{\partial f}{\partial t}\right)_{e-ph} = \frac{C_{ep}}{\sqrt{E}} \frac{\partial}{\partial E} \left[f(1-f) + k_B T_L(t) \frac{\partial f}{\partial E} \right], \quad (15)$$

where $C_{ep} = \pi^2 \hbar^3 G / \sqrt{2} k_B m_e^{3/2}$ and G is e - ph interaction constant. By substituting Eq. (15) into (13) we obtain the rate equation for the lattice temperature,

$$C_L \frac{\partial T_L}{\partial t} = G(T_e^* - T_L) + S_{GL}(t), \quad (16)$$

where

$$T_e^*(t) = \int dE f(E, t) [1 - f(E, t)] \quad (17)$$

plays the role of *effective* temperature of *athermal* electrons. Note that for thermal electron distribution f_0 , T_e^* coincides with the “regular” electron temperature T_e . The last term in Eq. (16) is added to describe heat exchange between the metal film and the glass substrate. With boundary conditions that the temperature and heat flux are continuous across the metal/glass interface, it has the form²¹: $S_{GL}(t) = \kappa_G \partial T_G / \partial z$, where T_G and κ_G are the glass temperature and thermal conductivity, respectively ($\kappa_G = 1.37$ J/mK for SiO₂). The above system should be supplemented by equation for heat transport in the glass,

$$C_G \frac{\partial T_G}{\partial t} = \kappa_G \frac{\partial^2 T_G}{\partial z^2}, \quad (18)$$

where C_G is the glass heat capacity ($C_G = 1.63 \times 10^7$ J/m²K for SiO₂). Note, however, that metal/glass dynamics is important only for long times (see below).

In the case short-time dynamics, the evolution of lattice temperature $T_L(t)$ is governed by the interaction with strongly athermal electrons gas, and thus requires solution of Boltzmann equation for e - ph system (14-16). We use the integral form for the e - e scattering term for parabolic band²⁰,

$$\left(\frac{\partial f}{\partial t}\right)_{e-e} = \frac{K_{ee}}{E_s^{3/2} E^{1/2}} \int dE_1 \int dE_2 F(E_1, E_2, E_3) \times \left[\frac{\sqrt{x}}{1+x} + \arctan \sqrt{x} \right]_{x_{min}}^{x_{max}}, \quad (19)$$

where $K_{ee} = m_e e^4 / (4\hbar^3 \varepsilon^2)$, ε is static dielectric constant of metal, and $E_s = (e^2 / 2\pi\varepsilon) (3n_e / \pi)^{1/3}$ is the Thomas-Fermi energy. The phase space for scattering is determined by $F(E_1, E_2, E_3) = \tilde{f}(E) \tilde{f}(E_1) f(E_2) f(E_3) - f(E) f(E_1) \tilde{f}(E_2) \tilde{f}(E_3)$, where $\tilde{f}(E) = 1 - f(E)$ and $E_3 = E + E_1 - E_2$, while the angular integrals of Coulomb interaction yield the expression in the brackets in the integrand which is evaluated between the limits: $x_{min, max} = \max, \min \left[(\sqrt{E_1} \mp \sqrt{E_3})^2, (\sqrt{E} \mp \sqrt{E_2})^2 \right] / E_s$. The last term in Eq. (14), describing the energy deposited

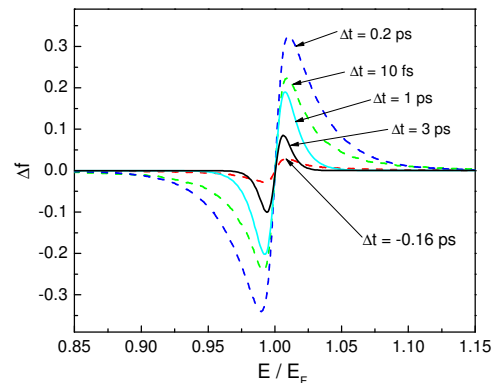


FIG. 5: Non-equilibrium contribution to the electron distribution function in Al film is shown for several time delays. Calculations are based on solution of the Boltzmann equation for the electron distribution function in Sec. III B.

by the pump pulse, is given by $H(E, t) = Q(E)S(t)$ with Gaussian pulse profile

$$S(t) = \frac{E_0}{\sqrt{\pi}\sigma_L} e^{-t^2/\sigma_L^2}, \quad (20)$$

where E_0 is the absorbed pump pulse energy density and $\sigma_L = 100$ fs is the pulsewidth. The factor $Q(E)$, describing the phase space of phonon-assisted electronic transitions after absorption of a photon with energy ω , is available in the literature²⁰ and is included in the numerical calculations.

In Fig. 5, we plot the time-dependent contribution to the electron distribution function, $\Delta f(E, t) = f(E, t) - f_0(E)$, versus energy (measured from the Fermi level) at several time delays. For short times, electron distribution is strongly non-equilibrium, as indicated by the long high-energy tail of Δf . At $t \sim 1$ ps, electrons are almost thermalized and their distribution is close to the Fermi function of a hot electron gas. Note that, at 1 ps, the magnitude of Δf has decreased significantly pointing to the energy transfer from electron gas to the lattice.

IV. DISCUSSION

The transient change in the lattice temperature, $T_L(t)$, provides the main contribution to the time-modulation of metal dielectric function,

$$\delta\varepsilon_m(\omega, t) = \frac{i\omega_p^2}{\omega(\omega + i\gamma_0)^2} [\gamma(T_L(t)) - \gamma_0], \quad (21)$$

where $\gamma(\omega, T_L)$ is the optical relaxation rate of an electron-hole pair excited by the probe light²² (γ_0 stands for the room-temperature relaxation rate). In the case when the lattice temperature remains much smaller than ω , the relaxation rate is nearly ω -independent¹⁷, and is given by

$$\gamma(T) = B \left(\frac{T_L}{\Theta_D} \right)^5 J \left(\frac{\Theta_D}{T_L} \right), \quad (22)$$

where $J(y) = \frac{1}{2} \int_0^y dx x^4 \coth \frac{x}{2}$, and B is a material-dependent constant. In the relevant temperature range $T_L \sim \Theta_D$, the T_L -dependence of γ is nearly linear, $\gamma(T_L) \approx \gamma_0 + \frac{B}{2}(T_L - T_0)$. Note that γ_0 contains contributions also from the electron-impurity and e - e scattering processes; however those are not significantly affected by the pump pulse due to a relatively small change in the scattering phase space by the fraction of photoexcited electrons.

The results of numerical simulations of short-time dynamics are shown in Fig. 2. The calculated differential transmission dT/T is in excellent agreement with the data, reproducing the signal rise at subpicosecond times. In Fig. 6 we show the evolution of the lattice temperature and the effective electron temperature. The rapid drop of T_e^* after reaching its peak value at ~ 200 fs is accompanied by increase in T_L during the period $t \lesssim 1$ ps, indicating energy intake by the phonon subsystem while the electron gas is still in the thermalization stage. After electron and phonon subsystems equilibrate, the signal changes weakly (plateau) until the slower process of energy transfer to the glass substrate takes over, leading to the decay of pump-probe signal from the metal [see Fig. 3]. For long time delays, electron and phonon subsystems are in thermal equilibrium with each other, and the long-time dynamics is well described by the *two-temperature model* that incorporates the heat exchange between the metal and the glass²¹. To compare to Boltzmann equation approach, here we also included in calculations the rate equation for electron temperature $T_e(t)$ that can be straightforwardly obtained from Eqs. (14-16) by the replacement of $f(E, t)$ with thermal distribution:

$$C_e \partial T_e / \partial t = G(T_L - T_e) + S(t), \quad (23)$$

where $C_e = \beta T_e$ (with $\beta = 134 \text{ J m}^{-3} \text{ K}^{-2}$ for Al) is the electronic heat capacity. After ~ 40 ps, the signal reaches a plateau corresponding to thermal equilibrium between film and glass [see Fig. 3]. Here the evolution of dT/T also follows mainly the phonon dynamics [see Fig. 6(b)]. Note, however, that the subpicosecond signal rise is noticeably faster than the one calculated using Boltzmann equation approach [cf. Fig. 2]. The reason is that thermal distribution overestimates the fraction of lower energy electrons and, hence, the rate of their energy transfer to the lattice. The measured signal also exhibits weak oscillations with a period ~ 5 ps; those could be attributed to the vibrational mode across the film that is excited by the rapid heating of the lattice, but are not captured by the present model.

The calculated transient spectra are shown in Fig. 4 for several time delays in the long-time regime when the electron and phonon subsystems are in thermal equilibrium with each other. The blueshift is well reproduced as well as is the nonlinear ω -dependence of dT/T in the main transmission band frequency range. The origin of the blueshift can be understood as follows. The eigenmodes in a nanohole array are the result of interference of multiple waves scattered from periodic metal/dielectric regions

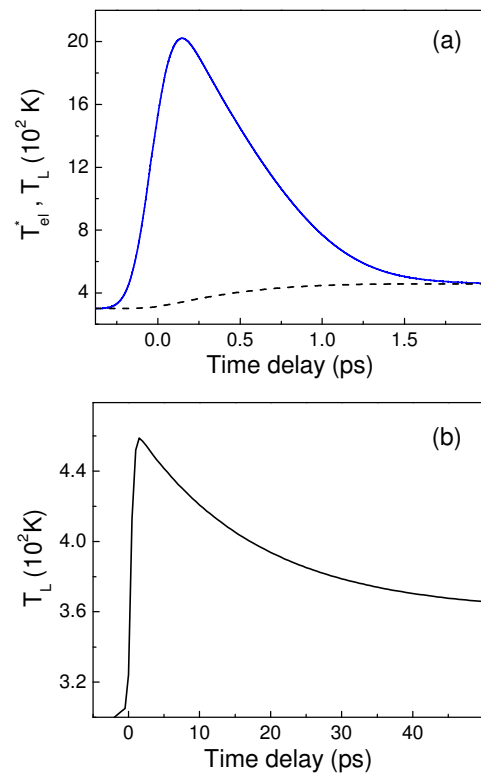


FIG. 6: (a) Short-time evolution of effective electron (solid line) and lattice (dashed line) temperatures in Al film following the excitation. (b) Long-time evolution of the lattice temperature due to heat transfer to the glass matrix.

as described by the above effective medium model. In the presence of *attenuation*, the phase of scattered wave has a contribution $\propto \text{Re}\sqrt{\varepsilon_m} = \varepsilon_m'' / \sqrt{|\varepsilon_m'|} \approx \gamma\omega_p/\omega^2$. Therefore, a transient change in attenuation causes corresponding shifts in scattering phases. This, in turn, changes the interference of waves making up an eigenmode. To compensate for the phase shifts, a transient increase in γ must be accompanied by a corresponding increase in ω ; and consequently the transmission resonances blueshift.

V. CONCLUSION

In summary, we investigated the ultrafast dynamics of Al-based plasmonic lattice that reveals a non-trivial role played by the plasma attenuation in determining the EOT resonant bands. While its effect on the SPP dispersion is relatively weak, attenuation is more important for modes comprised of a multitude of scattered waves. By directly altering their interference, ultrafast time-resolved optical techniques unravel the unique properties of photoexcited SEW in plasmonic metals.

This work was supported in part by NSF DMR Grant No. 05-03172, by NSF Grant No. DMR-0606509, and by NIH Grant No. 2 S06 GM008047-33.

-
- ¹ H. Raether, *Surface Plasmons on Smooth and Rough Surfaces and on Gratings*, (Springer-Verlag, Berlin, 1988).
- ² T. W. Ebbesen, H. J. Lezec, H. F. Ghaemi, T. Thio, and H. J. Wolff, *Nature (London)* **391**, 667 (1998).
- ³ U. Schröter and D. Heitmann, *Phys. Rev. B* **58**, 15419 (1998).
- ⁴ H. F. Ghaemi, T. Thio, D. E. Grupp, T. W. Ebbesen, and H. J. Lezec, *Phys. Rev. B* **58**, 6779 (1998).
- ⁵ L. Martín-Moreno, F. J. García-Vidal, H. J. Lezec, K. M. Pellerin, T. Thio, J. B. Pendry, and T. W. Ebbesen, *Phys. Rev. Lett.* **86**, 1114 (2001).
- ⁶ W. L. Barnes, A. Dereux, and T. W. Ebbesen, *Nature (London)* **424**, 824 (2003).
- ⁷ J. A. Porto, F. J. García-Vidal, and J. B. Pendry, *Phys. Rev. Lett.* **83**, 2845 (1999).
- ⁸ F. J. García-Vidal, H. J. Lezec, T. W. Ebbesen, and L. Martín-Moreno, *Phys. Rev. Lett.* **90**, 213901 (2003).
- ⁹ Ph. Lalanne, J. P. Hugonin, S. Astilean, M. Palamaru and K. D. Möller, *J. Opt. A* **2**, 48 (2000).
- ¹⁰ M. M. J. Treacy, *Appl. Phys. Lett.* **75**, 606-608 (1999).
- ¹¹ M. J. Treacy, *Phys. Rev. B* **66**, 195105 (2002).
- ¹² H. J. Lezec, and T. Thio, *Optics Express* **12**, 3629 (2004).
- ¹³ M. Tong, A. S. Kirakosyan, T. V. Shahbazyan, and Z. V. Vardeny, *Phys. Rev. Lett.* **100**, 056808 (2008).
- ¹⁴ C.-K. Sun, F. Vallée, L. H. Acioli, E. P. Ippen, J. G. Fujimoto, *Phys. Rev. B* **50**, 15337 (1994).
- ¹⁵ R. H. M. Groeneveld, R. Sprik, A. Lagenijk, *Phys. Rev. B* **51**, 11433 (1995).
- ¹⁶ D. Y. Smith, E. Shiles, and M. Inokuti, *The optical properties of metallic Aluminum*, in *Handbook of optical constant of solids*, Edited by E. D. Palik (Academic Press, 1985).
- ¹⁷ J. B. Smith, H. Ehrenreich, *Phys. Rev. B* **25**, 923 (1982).
- ¹⁸ B. Rethfeld, A. Kaiser, M. Vicanek, and G. Simon, *Phys. Rev. B* **65**, 214303 (2002).
- ¹⁹ S. A. Darmanyany and A. V. Zayats, *Phys. Rev. B* **67**, 035424, (2003).
- ²⁰ N. Del Fatti, C. Voisin, M. Achermann, S. Tzortzakis, D. Christofilos, and F. Vallée, *Phys. Rev. B* **61**, 16956 (2000).
- ²¹ P. Grua, J. P. Morreeuw, H. Bercegol, G. Jonusauskas and F. Vallée *Phys. Rev. B* **68**, 035424 (2003).
- ²² W. Götze and P. Wölfle, *Phys. Rev. B* **6**, 1226 (1972).